

# All-weather thermochromic windows for synchronous solar and thermal radiation regulation

Chongjia Lin<sup>1†</sup>, Jun Hur<sup>1†</sup>, Christopher Y. H. Chao<sup>2</sup>, Gongze Liu<sup>1</sup>, Shuhuai Yao<sup>1\*</sup>, Weihong Li<sup>1,3\*</sup>, Baoling Huang<sup>1,4\*‡</sup>

Adaptive control of solar and thermal radiation through windows is of pivotal importance for building energy saving. However, such synchronous passive regulations are challenging to be integrated into one thermochromic window. Here, we develop a solar and thermal regulatory (STR) window by integrating poly(*N*-isopropylacrylamide) (pNIPAm) and silver nanowires (AgNWs) into pNIPAm/AgNW composites. A hitherto unexplored mechanism, originating from the temperature-triggered water capture and release due to pNIPAm phase transition, is exploited to achieve simultaneous regulations of solar transmission and thermal emission. The STR window shows excellent solar modulation (58.4%) and thermal modulation (57.1%) and demonstrates effective regulation of indoor temperatures during both daytime and nighttime. Compared to other thermochromic technologies, the STR window reduces heat loss in cold environment while promotes heat dissipation in hot conditions, achieving efficient energy saving in all weathers. This dual solar and thermal regulation mechanism may provide unidentified insights into the advancement of smart window technology.

## INTRODUCTION

Carbon neutrality before 2050 is becoming a global consensus, and more than 110 countries have committed to a diversity of measures to improve energy efficiency and reduce carbon emissions (1). Building accounts for 30 to 40% of the total energy consumption, while around half of building energy is used for heating, ventilation, and air conditioning (2). Windows represent the major source of heat gain or loss as well as of visual and thermal discomfort and are regarded as the least energy-efficient sector of building envelope. Therefore, pursuing smart windows that dynamically adapt to variations of solar irradiance and weather conditions is essential for improving building energy efficiency (3). To achieve optimal energy regulation, two types of radiative heat flux should be considered: the solar radiation from the sun and the thermal radiation from objects (4). In the cold seasons, an ideal smart window should have high solar transmittance for external solar harvesting and low thermal emittance for internal heat insulation, whereas in the hot seasons, the window should have low solar transmittance for external solar blockage and high thermal emittance for internal heat dissipation. In particular, the thermal emittance regulation overwhelms the solar regulation in energy saving due to the round-the-clock thermal heat exchange between indoor space and surrounding environments, while the sunlight only exists for a partial time of a day. The estimated energy savings from an ideal thermal control window are 2.5 and 9 times of that from an ideal solar control window in summer and winter, respectively (5). Besides, the optical switch between different states can be stimulated from thermo-, electro-, photo- or

mechanoresponses (2). Among them, thermochromic windows by spectrum regulation according to the environmental temperature match the switching demands in cold and hot weather, therefore offering the great potential of energy saving (2–6).

However, most of the state-of-the-art thermochromic windows can only regulate solar radiation. Vanadium dioxide ( $\text{VO}_2$ ) and hydrogel are the two most widely investigated materials for thermochromic windows (6, 7).  $\text{VO}_2$  is infrared-transparent in the semiconducting state at low temperatures and infrared-reflective in the metallic state at high temperatures. It matches the demand of near-infrared (NIR) regulation, a part of solar radiation regulation, for thermochromic windows (8–10). Although coating  $\text{VO}_2$  on glass can generate thermal emittance regulation in the long-wavelength infrared, it is unfavorable regulation as the emittance is high at low temperatures while low at high temperatures, which is called as negative thermal regulation (11–15). The coating on metals reverses the optical behavior and achieves positive thermal regulation (the emittance is high at high temperature), but it makes the regulator opaque and unsuitable for windows (16). Thus, only the NIR regulation of  $\text{VO}_2$  has been widely used for thermochromic windows. It is worth mentioning that Wang *et al.* creatively coated a  $\text{VO}_2$  layer on a low-E film that has high reflectance (same as metal) on thermal range and high transmittance on visible range. It leads to a positive thermal regulation of 40% and a solar regulation of 9.3% (17). Hydrogel is another promising material for smart windows (18–20). It has high solar transmittance at low temperatures because of the index matching between the polymer and water. Beyond a critical temperature, the phase separation of hydrogel generates strong internal scattering and leads to low solar transmittance. Because of its spectrum modulation includes visible and NIR radiation, it has stronger solar regulation and consequently larger potential of energy saving than  $\text{VO}_2$  (20). Yet, the phase separation mechanism can only shape spectrum up to NIR, so it cannot fulfill the thermal radiation regulation. Only a combination of thermochromic and mechanical control has been used on a hydrogel-based window to realize solar and thermal regulation (21). Other materials, including ionic liquids, liquid crystals, and perovskites, were also explored for

<sup>1</sup>Department of Mechanical and Aerospace Engineering, The Hong Kong University of Science and Technology, Clear Water Bay, Kowloon, Hong Kong, China. <sup>2</sup>Department of Building Environment and Energy Engineering and Department of Mechanical Engineering, The Hong Kong Polytechnic University, Hong Kong, China. <sup>3</sup>Department of Mechanical Engineering, City University of Hong Kong, Kowloon, Hong Kong, China. <sup>4</sup>HKUST Shenzhen-Hong Kong Collaborative Innovation Research Institute, Futian, Shenzhen, China.

\*Corresponding author. Email: meshyao@ust.hk (S.Y.); weihongli6@cityu.edu.hk (W.L.); mebhhuang@ust.hk (B.H.)

†These authors contributed equally to this work.

‡Lead contact.

thermochromic windows, but they function only in visible and NIR regimes as well (2).

Here, we develop a solar and thermal regulatory thermochromic window (STR smart window) with an ultrabroadband positive regulation covering both solar and thermal spectra. It demonstrates competitive solar regulation ( $\Delta T_{\text{sol}} = 58.4\%$ ) and excellent positive thermal regulation ( $\Delta \epsilon = 57.1\%$ ) compared to the reported thermochromic regulators (Fig. 1A) (11–15, 17, 20–38). Its solar regulation is similar to the hydrogel window and around five times higher than a  $\text{VO}_2$  window. Meanwhile, its positive thermal regulation is comparable to a negative  $\text{VO}_2$  regulator and four times higher than a positive  $\text{VO}_2$  window. Besides, its high luminance transmittance ( $T_{\text{lum}} = 78.3\%$ ) and low transition temperature ( $\tau_c = 31^\circ\text{C}$ ) render it a promising smart window for enclosed spaces (e.g., windows in buildings or skylights in vehicles).

In the cold environment, the STR smart window has high solar transmittance ( $T_{\text{sol}} = 65.5\%$ ) for indoor solar heating in the daytime and high thermal reflectance ( $R_{\text{the}} = 64.8\%$ ) for indoor heat insulation

in both daytime and nighttime (Fig. 1, B<sub>1</sub> and B<sub>2</sub>). In the hot environment, the STR smart window shows low solar transmittance ( $T_{\text{sol}} = 7.1\%$ ) for alleviating indoor solar heating in the daytime and low thermal reflectance ( $R_{\text{the}} = 7.7\%$  or high thermal emission  $\epsilon = 92.3\%$ ) for facilitating indoor heat dissipation in both daytime and nighttime (Fig. 1, C<sub>1</sub> and C<sub>2</sub>).

## RESULTS

### Fabrication process and working mechanism

The STR smart window consists of a poly(*N*-isopropylacrylamide) (pNIPAm) hydrogel film grafting in a polydimethylsiloxane (PDMS) tray and a solar-transparent but thermal-reflective silver-nanowire (AgNW) mesh on the hydrogel film. When the temperature rises above the transition temperature, the pNIPAm undergoes a temperature-triggered phase separation and switch from solar transparent to opaque, providing solar modulation through the internal scattering (17). Simultaneously, because of the phase transition induced

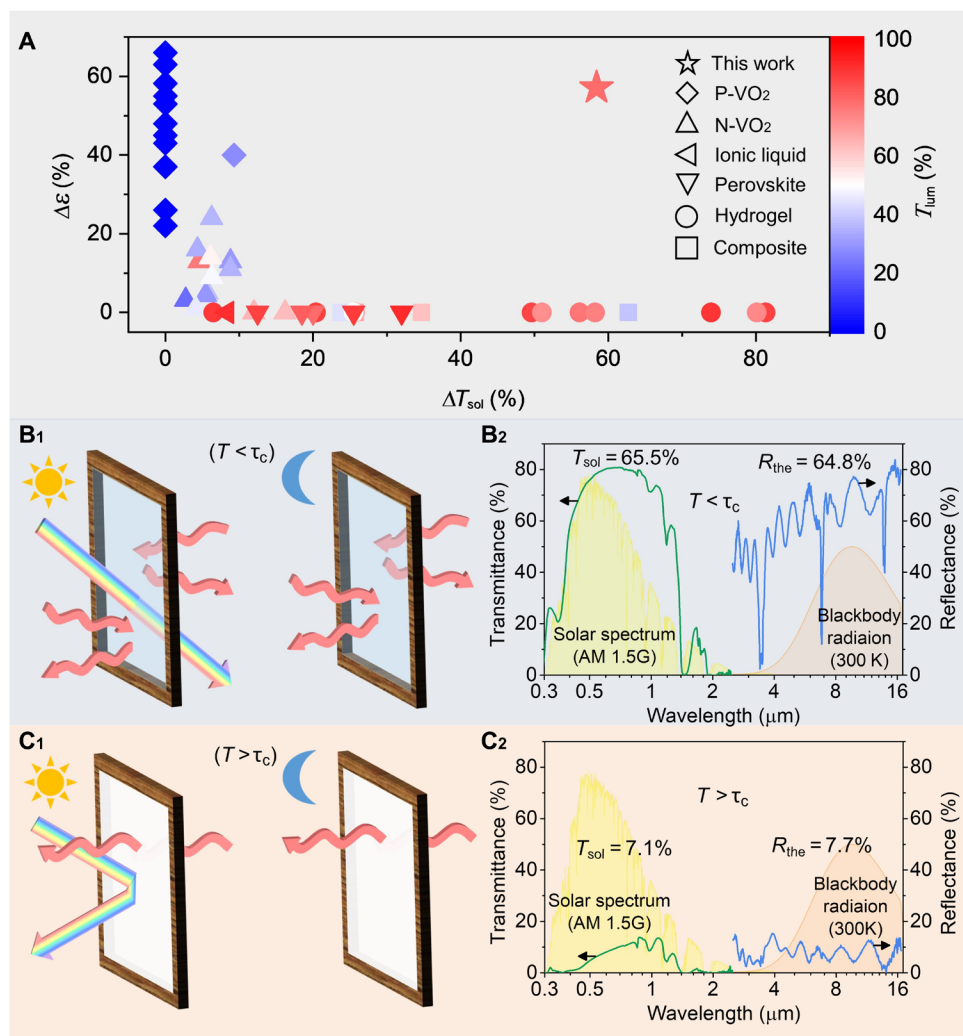


**Fig. 1. Thermochromic performance of the STR window.** (A) Thermochromic performance (solar transmittance modulation,  $\Delta T_{\text{sol}}$ ; thermal emittance modulation,  $\Delta \epsilon$ ; and luminance transmittance,  $T_{\text{lum}}$ ) in some of the best-reported smart materials (11–15, 17, 20–38). N- $\text{VO}_2$  and P- $\text{VO}_2$  represent the negative and positive thermal regulations of  $\text{VO}_2$ , respectively. (B<sub>1</sub> and B<sub>2</sub>) Schematic of optical performance in the cold condition (B<sub>1</sub>) and the corresponding spectrum (B<sub>2</sub>). (C<sub>1</sub> and C<sub>2</sub>) Schematic of optical performance in the hot condition (C<sub>1</sub>) and the corresponding spectrum (C<sub>2</sub>).

hydrophilic-to-hydrophobic conversion of the pNIPAm network, water molecules within the pNIPAm network are pumped out and cover the AgNW mesh. As water can strongly emit infrared radiation, the composite film switches from thermal reflective to emissive and enables thermal modulation.

The fabrication process of the STR smart window is illustrated in Fig. 2A. A PDMS tray was first cured and followed by pouring benzophenone solution [20 weight % (wt %) in acetone] into the tray. The benzophenone solution diffused into the PDMS network (see fig. S1) and facilitated the chemical bonds between PDMS and pNIPAm. The pNIPAm film was synthesized from a mixed solution of *N*-isopropylacrylamide (NIPAm), *N,N'*-methylenebis(acrylamide) (BIS), and ammonium persulfate (APS) initiator by free-radical polymerization within the PDMS tray, which was subsequently sealed by an AgNW-coated glass slide and stored in an ice-water bath. The polymerization lasted for 4 hours in an ultraviolet (UV) reactor with 340-nm UV light exposure and then 8 hours with UV light off. After polymerization, the pNIPAm hydrogel network was formed and grafted on the PDMS tray. This immobilized pNIPAm maintains the same transition temperature as the original pNIPAm, because the free radicals do not affect the hydrophobic and hydrophilic interaction between pNIPAm polymer chains and water molecules. Since NIPAm has stronger hydrophilic bonds than glass and the hydrophilic AgNWs are immersed in NIPAm solution, the AgNW mesh is easily transferred and embedded on the hydrogel top surface during the polymerization process. Last, after removing the glass slide, we enclosed the PDMS tray with a visible and infrared

transparent polyethylene (PE) film, which can be replaced by a variety of broadband-transparent optical sheets.

At low ambient temperature ( $T < \tau_c$ ), the pNIPAm cross-linked networks swell in water through intermolecular hydrophilic bonds (hydrogen bonds), and water molecules evenly disperse within the pNIPAm network (illustrated by the well-dispersed blue-dyed water in Fig. 2C). The refractive index of the water-rich polymer is close to that of water and thereby the hydrogel film is solar-transparent. The AgNW mesh deposited on top of the hydrogel film has high solar transmittance and high thermal reflectance (39). After integrating the hydrogel and AgNW mesh, the STR window exhibits high solar transmittance and thermal reflectance (low emissivity) (Fig. 2B) at low temperatures. When the temperature increases and exceeds the phase transition temperature ( $T > \tau_c$ ), hydrogen bonds are weakened, and the water/pNIPAm connecting structures are destroyed, triggering the hydrophobic associations and squeezing out water molecules. Since five sides of the pNIPAm network are chemically bonded with the PDMS tray, only the remaining free side of pNIPAm can shrink, resulting in directional water transportation and accumulation on top of the AgNW mesh (illustrated by the blue-dyed water accumulation on the free side in Fig. 2E). The phase separation and shrinkage of the pNIPAm network lead to polymer-rich and polymer-poor microphases, which generate light-scattering centers, turn the hydrogel to white, and efficiently reflect the sunlight (40). Figure S2 shows the thicker walls and bigger pore sizes after the phase separation of the pNIPAm. Moreover, the newly formed water layer has high thermal emissivity when its thickness is larger than 0.1 mm (see fig. S3) (41) and thereby suppresses the thermal reflection of the underlying AgNW mesh, providing notable thermal modulations (Fig. 2D). This STR smart window design realizes an excellent thermochromic function with synchronous modulation of solar and thermal radiation.

### Structural optimization and optical/thermal properties

The optical and thermal properties of the STR window are affected by the concentration of AgNW mesh, thickness of pNIPAm, and the concentration of BIS cross-linker. We change the concentration of AgNW mesh by varying the times of spin coating on glass slides (see fig. S4). The solar and thermal spectra of samples with one to three times of AgNW mesh spin coating are illustrated in Fig. 3A. The solar transmittance gradually decreases with the increasing concentration of AgNWs in the cold condition due to the minor solar reflection of the AgNW mesh (42, 43), whereas it maintains a small value (~7%) in the hot condition owing to the strong solar reflection of pNIPAm. The thermal reflectance is markedly enhanced by coating two times of AgNW mesh, and minor improvement is achieved for further AgNW deposition at low temperature. The variations of  $T_{\text{lum}}$ ,  $T_{\text{sol}}$ , and  $R_{\text{the}}$  are plotted in Fig. 3B. Overall, at low temperature, the luminance transmittance  $T_{\text{lum}}$  and solar modulation  $\Delta T_{\text{sol}}$  keep decreasing with a higher AgNW concentration, while the thermal reflectance increases markedly from 19.1 to 64.8% after twice AgNW deposition and becomes saturated thereafter. The variations of optical performance are smaller than 3 and 4% for solar and thermal regions, respectively. Therefore, a trade-off between solar transmittance and thermal modulation can be balanced by adjusting the amount of AgNWs.

The effects of pNIPAm thickness before and after coating AgNWs are illustrated in figs. S5 and S6. The luminance transmittance and thermal reflectance are not affected by the thickness of pNIPAm at

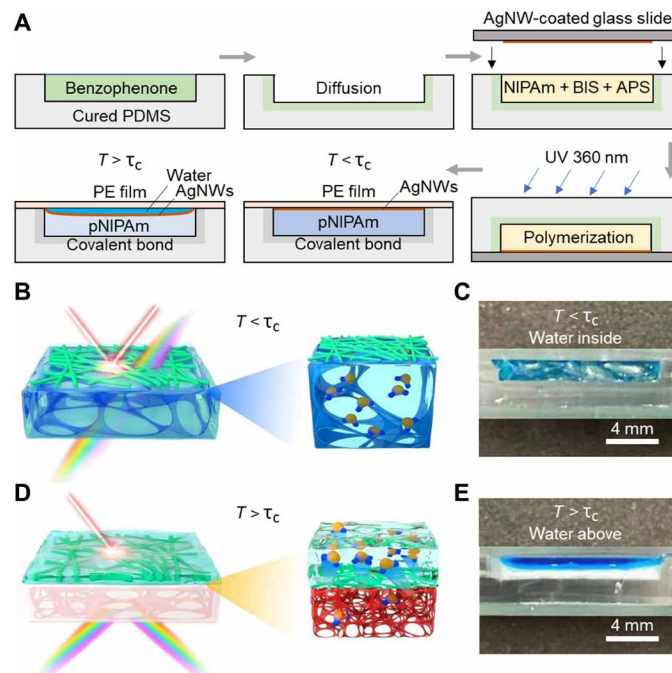


**Fig. 2. Fabrication process and working mechanism of the STR window.** (A) Fabrication process flow of the STR window. (B) Schematic of the working mechanism in the cold condition. (C) Image of the cross-sectional blue-dyed water distribution in the cold condition. (D) Schematic of the working mechanism in the hot condition. (E) Image of the cross-sectional blue-dyed water distribution in the hot condition.

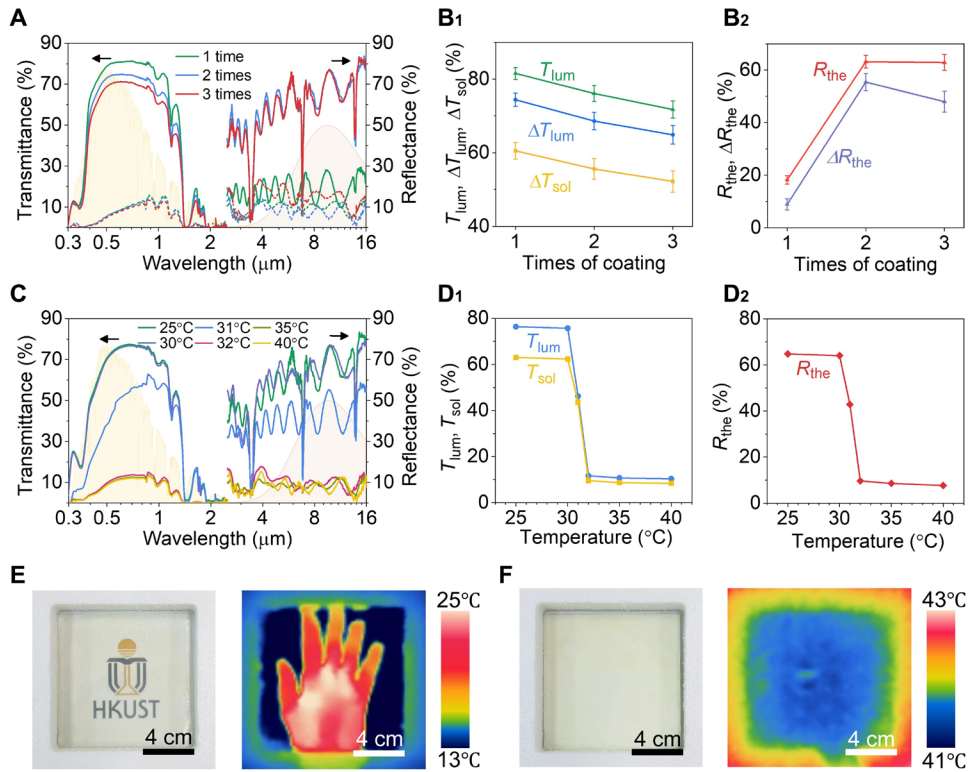


**Fig. 3. Optical and thermal properties of the STR window.** (A) Spectra of the STR windows with different times of AgNW coating. The solid and dashed lines represent the spectra in the cold and hot conditions, respectively. The orange and pink shadows represent the spectra of solar radiation (AM1.5G) and blackbody radiation (300 K), respectively. (B<sub>1</sub> and B<sub>2</sub>) Comparison of optical performance in terms of (B<sub>1</sub>) luminance transmittance ( $T_{\text{lum}}$ ), luminance transmittance modulation ( $\Delta T_{\text{lum}}$ ), and solar transmittance modulation ( $\Delta T_{\text{sol}}$ ) and (B<sub>2</sub>) thermal reflectance ( $R_{\text{the}}$ ) and thermal reflectance modulation ( $\Delta R_{\text{the}}$ ) of STR windows with different times of AgNW coating. (C) Spectra of the STR windows at different temperatures. The orange and pink shadows represent the spectra of solar radiation (AM1.5G) and blackbody radiation (300 K). (D<sub>1</sub> and D<sub>2</sub>) Comparison of optical performance in terms of (D<sub>1</sub>) luminance transmittance ( $T_{\text{lum}}$ ) and solar transmittance ( $T_{\text{sol}}$ ) and (D<sub>2</sub>) thermal reflectance ( $R_{\text{the}}$ ) of the STR window at different temperatures. (E) Visible and infrared images of the STR window in the cold condition. (F) Visible and infrared images of the STR window in the hot condition.

low temperature. However, the modulation of solar transmittance and thermal reflectance gradually grows with the increase of pNIPAm thickness. The concentration effect of the BIS cross-linker was also studied and shown in fig. S7. The composite film with 1% of BIS provides higher solar and thermal modulation than those with 0.25 and 0.5% of BIS. However, we noticed that the composite film with a BIS concentration higher than 1% cracked after heating-cooling cycling (see fig. S8). A higher BIS cross-linker concentration reduces the breaking strain, and thus, cracking is prone to occur once the residual stress during the heating-cooling cycles increases (44). Overall, we achieved an optimal STR window through an AgNW layer with two times of coating and a 2-mm-thick pNIPAm with BIS concentration of 1%, which would be used for later thermal management evaluation.

We further quantified the thermochromic property of the STR window by measuring the spectral properties at different temperatures. The solar transmittance and thermal reflectance are high when the hydrogel temperature is below the transition temperature ( $\tau_c$ ) of 31°C, while both of them drop to low values after phase separation occurs (Fig. 3C), resulting in solar and thermal modulation larger than 55% (Fig. 3D). Such ultrabroadband optical transformation can be demonstrated by the visible and infrared images with a 10 cm-by-10 cm STR window in the cold (Fig. 3E) and hot (Fig. 3F)

conditions. A colorful logo of HKUST could be seen clearly through the window at low temperature (Fig. 3E), while it was completely blocked at high temperature (Fig. 3F). Meanwhile, thermal radiation from a hand behind the infrared camera was reflected by the window in the cold condition (Fig. 3E) and absorbed in the hot condition (Fig. 3F).

#### Indoor temperature regulation tests

The optical and thermal properties of the STR window indicate excellent solar transmission and thermal radiation modulations. Here, we further quantified the indoor temperature regulation capabilities by monitoring the inner temperatures of four 12 cm by 12 cm by 15 cm chambers equipped with different types of windows (i.e., a glass window, commercial low-E window, hydrogel window and STR window with the same dimensions of 100 mm by 100 mm by 6 mm) under different environmental conditions (Fig. 4A and see fig. S9). The spectra and optical properties of other windows are shown in fig. S10 and table S1. The low-E window is widely used for energy saving in buildings and vehicles as it can selectively transmit visible light and reflect NIR light (45). The hydrogel window attracts enormous interest because of its excellent solar modulation capability (18). Other thermochromic windows, like VO<sub>2</sub>, were not used for comparison due to its poor performance in solar modulation.

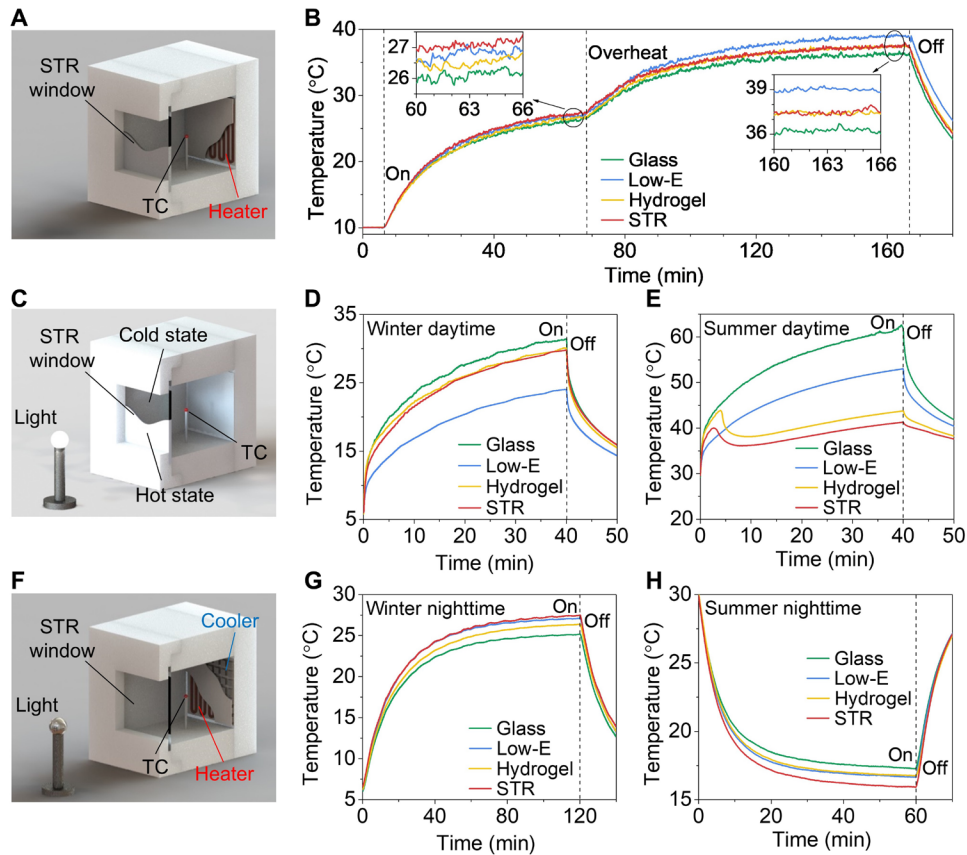


**Fig. 4. Thermal management tests of chambers with different windows.** (A) Schematic of the setup for the thermal-responsive tests. (B) Indoor air temperature histories of four chambers with two-stage indoor heating. (C) Schematic of the setup for daytime tests. (D) Indoor air temperature histories in simulated winter daytime. (E) Indoor air temperature histories in simulated summer daytime. (F) Schematic of the setup for nighttime tests. (G) Indoor air temperature histories in simulated winter nighttime. (H) Indoor air temperature histories in simulated summer nighttime. TC represents thermocouple in the setups.

We first measured the thermoresponsive behaviors of the tested windows by monitoring the indoor temperature versus time curves. Each chamber with an initial temperature of 10°C was heated by an internal heater (heating power = 3 W), and the internal air temperature was recorded (Fig. 4A). At the initial stage, the STR window was in the cold environment and had high thermal reflectance, thus providing the highest heat insulation capability (Fig. 4B). Specifically, the STR window illustrated better thermal insulation than the low-E window due to its lower thermal conductivity (or higher total thermal resistance) than low-E (see table S2). On the other hand, the glass and hydrogel windows led to slow temperature rises due to the lack of infrared reflecting capability. At the next stage, the heating power was increased to 5.2 W, and the chamber temperature continued rising to above 31°C, triggering the hydrogel phase transition. Subsequently, the STR window switched to the highly thermally emissive state and showed comparable heat dissipation capabilities to the hydrogel window. However, the low-E window retained invariable high thermal reflectance and produced an overheating of 1.8°C higher than the STR window. The smart temperature-responsive behaviors of our STR window demonstrate the superiority of the adaptive thermal reflectance and emissivity in regulating the indoor temperature. This heat insulation/dissipation switch can be triggered by not only internal heat loads (e.g., humans, heaters, or other indoor heat sources) but also external heat sources (e.g., sunlight) in applications.

We further used a solar simulator and controlled the ambient temperature to simulate weather conditions in winter and summer daytime (Fig. 4C) and quantified the window thermal management performance. In the winter daytime, the ambient temperature was set at 5°C, and the solar simulator (800 W/m<sup>2</sup>) was turned on to light the chamber (Fig. 4D). Comparing with the hydrogel window, the STR window has much higher thermal reflectance and provides better heat insulation capability, which compensates its lower solar energy gain due to lower solar transmission. Consequently, the temperatures of the STR and hydrogel chambers reached 30°C at 40 min, while the temperature of the low-E chamber was 6°C lower than that of the STR and hydrogel chambers due to its low solar transmission ( $T_{\text{sol}} = 38.6\%$  despite its high  $T_{\text{lum}} = 70\%$ ). The glass chamber showed slightly higher indoor temperature than both the STR and hydrogel chambers due to its highest solar transmission. In the summer daytime, the ambient temperature was set at 28°C, and the solar simulator power was 1000 W/m<sup>2</sup> (Fig. 4E). The temperatures of glass and low-E chambers increased monotonically above 60° and 50°C, respectively. In contrast, the temperatures of the hydrogel and STR chambers showed an increase-decrease trend because the phase transition occurring at around 3 to 4 min impeded further solar heating, and the chamber temperatures eventually were maintained under 45°C. In particular, owing to faster phase transition and lower solar transmission of the STR window, the temperature of the STR chamber was around 3°C lower than that of the hydrogel chamber.

Besides the daytime thermal management tests, we further measured the temperature response under conditions in the winter and summer nighttime. We installed a heater (silicone heating sheet with a heating power of 3 W) or a cooler (Peltier cooler with a cooling power of 13 W) on the backside of the chambers (Fig. 4F) and controlled the ambient temperature to simulate the heating in winter or cooling in summer. In the winter nighttime (the ambient temperature was 6°C), after the heater was turned on, the temperature of the STR chamber reached 27.5°C at 120 min, followed by the low-E chamber of 27°C (Fig. 4G), because both have high thermal reflectance and in turn similar thermal insulation capabilities. The temperatures of the hydrogel and glass chambers were 1.5° and 2.7°C lower than that of the STR chamber, because of their high thermal emissivity and thereby high heat loss from inside to outside. In the summer nighttime (the ambient temperature was 30°C), after the cooler was turned on to simulate air conditioning, the temperature of the STR chamber achieved the lowest value as its high thermal reflectance suppressed the heat transfer from the hot ambient to the cool chamber. The temperatures of the hydrogel and glass chambers were 1° to 2°C higher (Fig. 4H) due to their relatively higher thermal absorptance. The low-E chamber showed similar performance to that of the hydrogel chamber despite its high thermal reflectance, which was believed to be due to its higher thermal conductance. Overall, thanks to its adaptive and reversible switch from solar transparent to opaque and thermal reflective (heat insulation) to emissive (heat dissipation), the STR window realizes smart and excellent indoor temperature regulations for all weather conditions, i.e., winter daytime and nighttime as well as summer daytime and nighttime.

### Window durability and energy-saving simulations

The long-term durability of the window is of paramount importance for real applications. Although the pNIPAm network has a porous structure with different pore sizes at low and high temperatures, the change of pore size comes from the combination/separation of inner pores' walls, which will not lead to open holes on the top surface (see fig. S4). Thus, only water molecules can penetrate through the top surface, while AgNW mesh maintains a good coverage on top of pNIPAm, rendering the structure stable for long-term usage. We investigated the long-term durability of the STR window through heating-cooling cyclic tests of over 500 cycles in which each cycle consists of 1-min heating at 60°C and 3-min cooling at 20°C. The spectra of the window were measured every 100 cycles (see fig. S11). The  $T_{lum}$ ,  $\Delta T_{lum}$ , and  $\Delta T_{sol}$  showed less than 5% decrease after 500 cycles (Fig. 5A). The variations of the  $R_{the}$  and  $\Delta R_{the}$  were maintained within 10% (Fig. 5B). The present pNIPAm network structure remains unchanged and tightly clinging to the PDMS tray during the entire test (see movie S1). The immobilized pNIPAm maintains similar microstructure after hundreds of cycles (see figs. S2 and S12). These cycling tests demonstrate the excellent cyclic durability of the STR window.

Realizing smart indoor temperature regulation without HVAC (heating, ventilation and air-conditioning) systems is preferred for achieving building carbon neutrality. Here, we explored the indoor temperature regulation capacity of the STR window by EnergyPlus simulations, in comparison with three other types of windows mentioned before. The weather data of Beijing was selected because of its large annual temperature variation [temperature is often over 30°C in summer and below -8°C in winter (46)]. The energy consumption

of a one-floor house (see fig. S13) was obtained with the measured optical data (see table S1) of four different windows as input, while the internal heat loads were assumed to be from two people and from electrical and electronic devices inside the house (heat flux of 6 W/m<sup>2</sup>). The monthly average outdoor and indoor temperature with different windows are shown in figs. S14 (without internal heat loads) and S15 (with internal heat loads). In different seasons, the indoor temperature with standard glass window is always 3.5° to 6.5°C higher than outdoor temperature (see fig. S14) even without internal heat loads, which is caused by the solar irradiance heating and indoor heat-trapping effect. Correspondingly, the monthly indoor-outdoor temperature difference increases to 7° to 10°C when internal heat loads are considered (see fig. S15), indicating the greenhouse effect of enclosed spaces. Compared to the normal glass, the low-E window makes the room cooler in all seasons, while the hydrogel window produces cooling effects only in summer. In contrast, our STR window makes the room cooler in summer and warmer in winter. The temperatures during the tests with internal heat loads in four successive days in January and July are plotted in Fig. 5 (C and D). In January, STR, hydrogel, and glass windows illustrate similar temperatures in daytime, while low-E window has the lowest temperature due to its low solar transmittance. In nighttime, the temperature difference between STR and low-E windows remains unchanged due to their similar emittances, while that between STR and hydrogel/glass windows increase due to their different emittances. In July, owing to the low solar transmittance and high thermal emittance, STR window shows the lowest temperature in daytime, followed by hydrogel and low-E windows. The temperature differences among them in nighttime have similar trend to that in January, because of the same trend of surface emittances. Thanks to the ultrabroadband spectral modulation and thereby excellent temperature regulation capacity, the STR window provides the highest temperature in January while the lowest temperature in July no matter whether there are internal heat loads or not. The temperature regulation capacity of the hydrogel window is slightly lower than the STR window, while both are better than the glass window or low-E window.

Moreover, energy-saving calculations were performed with the indoor temperature controlled at 26°C by an HVAC system, which is an economic temperature recommended by the U.S. Department of Energy (47). Additional two windows (low-E and hydrogel windows) were compared with the STR window in terms of the monthly energy saving in Beijing (Fig. 5E). Unexpectedly, the low-E window produced positive energy savings in hot seasons while negative energy savings (energy consumptions) in cold seasons due to its high reflectance to near infrared radiation. The hydrogel window could save notable energy in hot seasons and showed no impact in cold seasons. However, the STR window achieved positive energy savings in all the seasons, specifically in winter and summer. Quantitatively, the total annual energy saving from the STR window is 6.8 times and 2.1 times more than the low-E and hydrogel windows in Beijing, respectively. Annual energy savings were also calculated for additional three cities: Anchorage, Hong Kong, and Abu Dhabi (Fig. 5F). Together with Beijing, we have simulated the cities in different climates, including high-latitude (Anchorage), mid-latitude (Beijing), subtropical (Hong Kong), and hot desert (Abu Dhabi) climates. Note that the STR window achieved remarkable energy savings in Anchorage, while the low-E and hydrogel windows provided near-zero energy savings because they lose functions in cold climate. As the latitudes decrease from Beijing to Abu Dhabi, the three windows provided

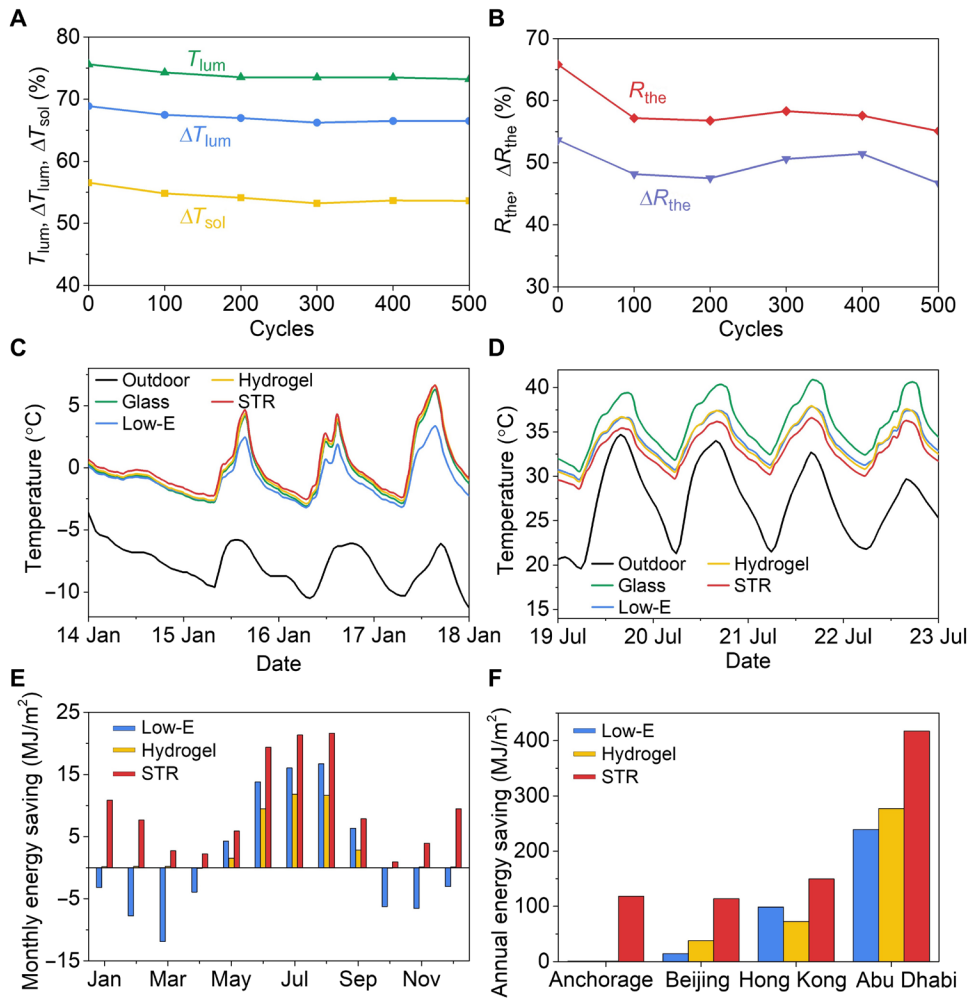


**Fig. 5. Stability and energy efficiency.** (A) Variations of luminance transmittance ( $T_{\text{lum}}$ ), luminance transmittance modulation ( $\Delta T_{\text{lum}}$ ), and solar transmittance modulation ( $\Delta T_{\text{sol}}$ ) with heating-cooling cycles. (B) Variations of thermal reflectance ( $R_{\text{the}}$ ) and thermal reflectance modulation ( $\Delta R_{\text{the}}$ ) with heating-cooling cycles. (C) Indoor temperature histories with different windows within four successive days in January in Beijing. (D) Indoor temperature histories with different windows within four successive days in July in Beijing. (E) Monthly energy savings with different windows compared to the standard glass window in Beijing. (F) Annual energy savings with different windows compared to the standard glass window in four cities.

increasing annual energy savings, among which the STR window performed the best. Quantitatively, the STR window can save more than 100 MJ/m<sup>2</sup> in Anchorage, Beijing (double that of the low-E window), and Hong Kong and 400 MJ/m<sup>2</sup> in Abu Dhabi, showing its great energy-saving capacity for all-weather conditions.

## DISCUSSION

We propose an ultrabroadband thermochromic window (STR smart window) and demonstrate its excellent indoor temperature regulation capacity. We exploit a hitherto unexplored mechanism to achieve synchronous modulations of both solar and thermal radiation through a pNIPAm-AgNW mesh composite film. In particular, water molecules are used as a thermal regulator, and its directional transfer through the AgNW mesh is controlled by the thermally induced hydrophobic-hydrophilic transition of pNIPAm. The water transport enables thermal regulation, while the phase separation of pNIPAm allows solar regulation at different temperature

conditions. On the basis of this new mechanism, the STR smart window can manipulate an ultrabroadband spectral regulation with excellent solar transmittance modulation of 58.4% and thermal reflectance (emittance) modulation of 57.1%. Further, its high luminance transmittance (78.3%) and low transition temperature ( $\tau_c = 31^{\circ}\text{C}$ ) make it efficient and feasible in real applications. Different from all the reported smart windows that merely regulate solar irradiance transmission, the STR window manages the indoor temperature by regulating both solar and thermal radiations, enabling its temperature regulation in all-weather conditions. Compared with the normal glass, low-E, and hydrogel windows, STR window achieves lower indoor temperature in summer and higher indoor temperature in winter for both daytime and nighttime, based on which, the energy saving of HVAC systems has been estimated in four different cities: Anchorage, Beijing, Hong Kong, and Abu Dhabi through a house simulation. The results illustrate that STR window has positive energy saving in all cities. By contrast, the low-E and hydrogel windows reduce energy consumption only in hot climates. Because

this novel structure is exploited for thermochromic windows, some potential issues need to be investigated in the future. Antifreezing capability can be improved by mixing antifreezes to lower the freezing point and maintain the performance in cold regions. Water evaporation can be relieved by mixing a high-boiling solvent with water to reduce the evaporation rate or using a cover with low water vapor permeability to preserve water in hydrogel. The potential water leakage and uneven distribution in large panels can be prevented by using rigid optical films and gridding encapsulation. Other transparent polymers can also be used as the substitutes of the PDMS frame. This polymer frame-core design contributes to not only the directional movement of water but also the realization of an adhesive substrate on glass, which may easily fit to existing windows. This unprecedented technology may lead to new development of smart windows.

## MATERIALS AND METHODS

### Materials

NIPAm ( $\geq 99\%$ ), BIS ( $99\%$ ) cross-linker, APS ( $\geq 98\%$ ) initiator, benzophenone ( $99\%$ ), *N,N,N',N'*-tetramethylethylenediamine (TEMED;  $\sim 99\%$ ), and acetone ( $\geq 99.5\%$ ) were purchased from Sigma-Aldrich. Methanol ( $\geq 99.8\%$ ) was purchased from Scharlab. The SYLGARD 184 Silicone Elastomer Kit was purchased from DOW Corning. AgNW (ethanol, 30 wt %) was purchased from Gu's Nano Technology. All the reagents were used without further purification.

### Preparation of STR windows

The PDMS chamber was prepared by mixing the elastomer base and curing agent at a weight ratio of 10:1. The mixture was poured into a negative mold with dimensions of 140 mm by 140 mm by 4 mm. The negative mold is closed with a flat reference with 100 mm by 100 mm by 2 mm positive mold. The mold was placed in an oven and cured at  $70^\circ\text{C}$  for 3 hours. The PDMS chamber is then removed from the mold and submerged in benzophenone solution (20 wt % in acetone) for 15 min to allow the benzophenone diffuse through PDMS. The PDMS tray was rinsed with methanol and dried in a vacuum chamber. In addition, the AgNW solution in ethanol is diluted to 15 wt % and coated on 120 mm by 120 mm by 2 mm glass slides by spin coating at 2000 rpm.

The pNIPAm film was synthesized by free-radical polymerization with APS initiator and TEMED accelerator and grafted on PDMS by photoinitiated benzophenone under UV light. NIPAm (3.39 g) and BIS (49 mg) were dissolved in 30 ml of deionized water and purged with  $\text{N}_2$  for 20 min. The solution temperature was kept below  $10^\circ\text{C}$  in an ice water bath during the preparation and polymerization. The polymerization was initiated by adding 10 wt % APS (180  $\mu\text{l}$ ) initiator and TEMED (80  $\mu\text{l}$ ) accelerator to the monomer solution subsequently. The solution was instantly poured into the as-prepared PDMS chamber and sealed by the AgNW-coated glass slide. The chamber was stored in an ice-water bath, which was placed in a UV reactor (40-W lamp, 340-nm wavelength). The polymerization took 4 hours in the UV reactor and 8 hours without UV exposure. After polymerization, the glass slide was removed with the AgNW mesh successfully being transferred onto the hydrogel. Last, the pNIPAm film-grafted PDMS chamber was enclosed with a thin PE film.

### Characterization

The spectra in the solar range (0.25 to 2.5  $\mu\text{m}$ ) were measured by a UV-visible-NIR spectrometer (Lambda 950, PerkinElmer) equipped

with a 150-mm integrating sphere. The spectra in the thermal range (2.5 to 16  $\mu\text{m}$ ) were measured by a Fourier transform infrared spectrometer (Vertex 70, Bruker) with a gold-coated integrating sphere (PIKE Technologies). The morphologies of samples were observed by scanning electron microscopy (TM3030 Tabletop Microscope). The thermal conductivities of different materials were measured through a thermal conductivity meter (TPS 2500s).

The solar transmittance ( $T_{\text{sol}}$ ) and thermal reflectance ( $R_{\text{the}}$ ) are calculated as follows

$$T_{\text{sol}} = \frac{\int_{0.3 \mu\text{m}}^{2.5 \mu\text{m}} T(\lambda) E_{\text{sol}}(\lambda) d\lambda}{I_{\text{sol}}} \quad (1)$$

$$R_{\text{the}} = \frac{\int_{3 \mu\text{m}}^{16 \mu\text{m}} R(\lambda) E_{\text{bla}}(\lambda) d\lambda}{I_{\text{bla}}} \quad (2)$$

where  $T(\lambda)$  and  $R(\lambda)$  are the measured spectral transmittance and reflectance, respectively.  $E_{\text{sol}}(\lambda)$  and  $E_{\text{bla}}(\lambda)$  are the spectral solar power (AM1.5G) and spectral blackbody radiation power at 300 K, respectively.  $I_{\text{sol}}$  and  $I_{\text{bla}}$  are corresponding the total solar radiation and the total blackbody radiation, respectively. The luminance transmittance ( $T_{\text{lum}}$ ) is calculated as follows

$$T_{\text{lum}} = \frac{\int_{0.38 \mu\text{m}}^{0.78 \mu\text{m}} \phi(\lambda) T(\lambda) d\lambda}{\int_{0.38 \mu\text{m}}^{0.78 \mu\text{m}} \phi(\lambda) d\lambda} \quad (3)$$

where  $\phi(\lambda)$  is the standard luminous efficiency for vision.  $T(\lambda)$  is the same as above.

### Preparation of temperature management tests

Test chambers were constructed with white XPS (extruded polystyrene) sheets with a thickness of 5 cm. The inner space size of the chamber is 12 cm by 12 cm by 15 cm with a 10 cm by 10 cm opening to install different windows. A solar simulator (Oriel PVIV-212v) was used as the light source for daytime tests. A silicone heating sheet (10 cm by 10 cm) was attached as an internal heat load to the inner side of a back XPS wall. A Peltier cooler (10 cm by 10 cm) was attached as a cooler to the inner side of a back XPS wall. A T-type thermocouple was installed at the center of the chamber to measure the indoor air temperature. Two low-E glasses, including a solar control low-E glass with high visible transmittance (65%) and low solar transmittance (39%) and an online low-E glass with high thermal reflectance (70%), were used in the daytime and nighttime tests, respectively.

### Indoor thermal regulation and energy-saving simulations

An 8 m by 8 m by 3 m model house with four 2 m by 4 m windows in the center of four walls (see fig. S11) was built in EnergyPlus. Glass, low-E, hydrogel, and STR windows were calculated separately, with optical data shown in table S1 for the four windows. The internal heat loads were calculated on the basis of the house area (48). Two people and total power of 6  $\text{W}/\text{m}^2$  from electronic and electrical devices were considered as internal heat loads. Climate data of Anchorage, Beijing, Hong Kong, and Abu Dhabi were selected to analyze the window performance in different latitudes. The indoor thermal regulation by the smart windows was recorded through the simulation without an HVAC system, while the energy-saving assessment was proceeded by adding an HVAC system with a single

set point of 26°C and recording the energy consumption for both heating and cooling of each model.

## SUPPLEMENTARY MATERIALS

Supplementary material for this article is available at <https://science.org/doi/10.1126/sciadv.abn7359>

## REFERENCES AND NOTES

1. A. Guterres, Carbon neutrality by 2050: The world's most urgent mission (United Nations, 2020).
2. Y. Ke, J. Chen, G. Lin, S. Wang, Y. Zhou, J. Yin, P. S. Lee, Y. Long, Smart windows: Electro-, thermo-, mechano-, photochromics, and beyond. *Adv. Energy Mater.* **9**, 1902066 (2019).
3. M. Tarantini, A. D. Loprieno, P. L. Porta, A life cycle approach to Green Public Procurement of building materials and elements: A case study on windows. *Energy* **36**, 2473–2482 (2011).
4. L. Long, H. Ye, How to be smart and energy efficient: A general discussion on thermochromic windows. *Sci. Rep.* **4**, 6427 (2014).
5. H. Ye, X. Meng, B. Xu, Theoretical discussions of perfect window, ideal near infrared solar spectrum regulating window and current thermochromic window. *Energ. Buildings* **49**, 164–172 (2012).
6. R. Baetens, B. P. Jelle, A. Gustavsen, Properties, requirements and possibilities of smart windows for dynamic daylight and solar energy control in buildings: A state-of-the-art review. *Sol. Energy Mater. Solar Cells* **94**, 87–105 (2010).
7. Y. Ke, C. Zhou, Y. Zhou, S. Wang, S. H. Chan, Y. Long, Emerging thermal-responsive materials and integrated techniques targeting the energy-efficient smart window application. *Adv. Funct. Mater.* **28**, 1800113 (2018).
8. S. M. Babulanam, T. S. Eriksson, G. A. Niklasson, C. G. Granqvist, Thermochromic VO<sub>2</sub> films for energy-efficient windows. *Sol. Energy Mater.* **16**, 347–363 (1987).
9. Y. Cui, Y. Ke, C. Liu, Z. Chen, N. Wang, L. Zhang, Y. Zhou, S. Wang, Y. Gao, Y. Long, Thermochromic VO<sub>2</sub> for energy-efficient smart windows. *Joule* **2**, 1707–1746 (2018).
10. Y. Ke, Y. Yin, Q. Zhang, Y. Tan, P. Hu, S. Wang, Y. Tang, Y. Zhou, X. Wen, S. Wu, T. J. White, J. Yin, J. Peng, Q. Xiong, D. Zhao, Y. Long, Adaptive thermochromic windows from active plasmonic elastomers. *Joule* **3**, 858–871 (2019).
11. J. Du, Y. Gao, Z. Chen, L. Kang, Z. Zhang, H. Luo, Enhancing thermochromic performance of VO<sub>2</sub> films via increased microroughness by phase separation. *Sol. Energy Mater. Sol. Cells* **110**, 1–7 (2013).
12. L. Kang, Y. Gao, Z. Chen, J. du, Z. Zhang, H. Luo, Pt/VO<sub>2</sub> double-layered films combining thermochromic properties with low emissivity. *Sol. Energy Mater. Sol. Cells* **94**, 2078–2084 (2010).
13. L. Kang, Y. Gao, H. Luo, J. Wang, B. Zhu, Z. Zhang, J. du, M. Kanehira, Y. Zhang, Thermochromic properties and low emissivity of ZnO: Al/VO<sub>2</sub> double-layered films with a lowered phase transition temperature. *Sol. Energy Mater. Sol. Cells* **95**, 3189–3194 (2011).
14. Z. Zhang, Y. Gao, Z. Chen, J. du, C. Cao, L. Kang, H. Luo, Thermochromic VO<sub>2</sub> thin films: Solution-based processing, improved optical properties, and lowered phase transformation temperature. *Langmuir* **26**, 10738–10744 (2010).
15. Z. Zhang, Y. Gao, H. Luo, L. Kang, Z. Chen, J. du, M. Kanehira, Y. Zhang, Z. L. Wang, Solution-based fabrication of vanadium dioxide on F:SnO<sub>2</sub> substrates with largely enhanced thermochromism and low-emissivity for energy-saving applications. *Energ. Environ. Sci.* **4**, 4290–4297 (2011).
16. H. Wei, J. Gu, F. Ren, L. Zhang, G. Xu, B. Wang, S. Song, J. Zhao, S. Dou, Y. Li, Smart materials for dynamic thermal radiation regulation. *Small* **1**, 2100446 (2021).
17. S. Wang, T. Jiang, Y. Meng, R. Yang, G. Tan, Y. Long, Scalable thermochromic smart windows with passive radiative cooling regulation. *Science* **374**, 1501–1504 (2021).
18. Y. Zhou, X. Dong, Y. Mi, F. Fan, Q. Xu, H. Zhao, S. Wang, Y. Long, Hydrogel smart windows. *J. Mater. Chem. A* **8**, 10007–10025 (2020).
19. Y. Zhou, S. Wang, J. Peng, Y. Tan, C. Li, F. Y. C. Boey, Y. Long, Liquid thermo-responsive smart window derived from hydrogel. *Joule* **4**, 2458–2474 (2020).
20. X. Li, C. Liu, S. Feng, N. X. Fang, Broadband light management with thermochromic hydrogel microparticles for smart windows. *Joule* **3**, 290–302 (2019).
21. S. Wang, Y. Zhou, T. Jiang, R. Yang, G. Tan, Y. Long, Thermochromic smart windows with highly regulated radiative cooling and solar transmission. *Nano Energy* **89**, 106440 (2021).
22. R. Beaini, B. Baloukas, S. Loquai, J. E. Klemburg-Sapieha, L. Martinu, Thermochromic VO<sub>2</sub>-based smart radiator devices with ultralow refractive index cavities for increased performance. *Sol. Energy Mater. Sol. Cells* **205**, 110260 (2020).
23. D. Cao, C. Xu, W. Lu, C. Qin, S. Cheng, Sunlight-driven photo-thermochromic smart windows. *Solar RRL* **2**, 1700219 (2018).
24. E. Haddad, R. V. Kruselecky, A. Hendaoui, M. Chaker, W. Jamroz, P. Poinas, Large tuneability IR emittance thermal control coating for space applications, in *43rd International Conference on Environmental Systems*, p. 3436.
25. Y.-S. Yang, Y. Zhou, F. B. Y. Chiang, Y. Long, Temperature-responsive hydroxypropylcellulose based thermochromic material and its smart window application. *RSC Adv.* **6**, 61449–61453 (2016).
26. K. Ito, T. Watari, K. Nishikawa, H. Yoshimoto, H. Iizuka, Inverting the thermal radiative contrast of vanadium dioxide by metasurfaces based on localized gap-plasmons. *APL Photonics* **3**, 086101 (2018).
27. A. M. Morsy, M. T. Barako, V. Jankovic, V. D. Wheeler, M. W. Knight, G. T. Papadakis, L. A. Sweatlock, P. W. C. Hon, M. L. Povinelli, Experimental demonstration of dynamic thermal regulation using vanadium dioxide thin films. *Sci. Rep.* **10**, 13964 (2020).
28. M. Ono, K. Chen, W. Li, S. Fan, Self-adaptive radiative cooling based on phase change materials. *Opt. Express* **26**, A777–A787 (2018).
29. K. Sun, C. A. Riedel, A. Urbani, M. Simeoni, S. Mengali, M. Zalkovskij, B. Bilenberg, C. H. de Groot, O. L. Muskens, VO<sub>2</sub> thermochromic metamaterial-based smart optical solar reflector. *ACS Photonics* **5**, 2280–2286 (2018).
30. X. Wang, Y. Cao, Y. Zhang, L. Yan, Y. Li, Fabrication of VO<sub>2</sub>-based multilayer structure with variable emittance. *Appl. Surf. Sci.* **344**, 230–235 (2015).
31. Z. Xu, S. Wang, X.-Y. Hu, J. Jiang, X. Sun, L. Wang, Sunlight-induced photo-thermochromic supramolecular nanocomposite hydrogel film for energy-saving smart window. *Solar RRL* **2**, 1800204 (2018).
32. Y. Zhou, Y. Cai, X. Hu, Y. Long, Temperature-responsive hydrogel with ultra-large solar modulation and high luminous transmission for “smart window” applications. *J. Mater. Chem. A* **2**, 13550–13555 (2014).
33. Y. Zhou, Y. Cai, X. Hu, Y. Long, VO<sub>2</sub>/hydrogel hybrid nanothermochromic material with ultra-high solar modulation and luminous transmission. *J. Mater. Chem. A* **3**, 1121–1126 (2015).
34. Y. Zhou, M. Layani, F. Y. C. Boey, I. Sokolov, S. Magdassi, Y. Long, Electro-thermochromic devices composed of self-assembled transparent electrodes and hydrogels. *Adv. Mater. Technol.* **1**, 1600069 (2016).
35. Y. Zhou, M. Layani, S. Wang, P. Hu, Y. Ke, S. Magdassi, Y. Long, Fully printed flexible smart hybrid hydrogels. *Adv. Funct. Mater.* **28**, 1705365 (2018).
36. Y. Zhu, H. Qian, R. Yang, D. Zhao, Radiative sky cooling potential maps of China based on atmospheric spectral emissivity. *Sol. Energy* **218**, 195–210 (2021).
37. J. Zhu, A. Huang, H. Ma, Y. Ma, K. Tong, S. Ji, S. Bao, X. Cao, P. Jin, Composite film of vanadium dioxide nanoparticles and ionic liquid-nickel-chlorine complexes with excellent visible thermochromic performance. *ACS Appl. Mater. Interfaces* **8**, 29742–29748 (2016).
38. Y. Zhang, C. Y. Tso, J. S. Iñigo, S. Liu, H. Miyazaki, C. Y. H. Chao, K. M. Yu, Perovskite thermochromic smart window: Advanced optical properties and low transition temperature. *Appl. Energy* **254**, 113690 (2019).
39. T. Li, Y. Gao, K. Zheng, Y. Ma, D. Ding, H. Zhang, Achieving better greenhouse effect than glass: Visibly transparent and low emissivity metal-polymer hybrid metamaterials. *ES Energy Environ.* **5**, 102–107 (2019).
40. A. Eklund, H. Zhang, H. Zeng, A. Priimagi, O. Ikkala, Fast switching of bright whiteness in channeled hydrogel networks. *Adv. Funct. Mater.* **30**, 2000754 (2020).
41. M. Vollmer, K. Möllmann, *Infrared Thermal Imaging: Fundamentals, Research and Applications* (John Wiley & Sons, 2017).
42. T. Tomiyama, I. Mukai, H. Yamazaki, Y. Takeda, Optical properties of silver nanowire/polymer composite films: Absorption, scattering, and color difference. *Opt. Mater. Express* **10**, 3202–3214 (2020).
43. Silver nanowires: A new nanomaterial with advances for electrical, optical and IR systems (International Society for Optics and Photonics, 2019).
44. J. Liu, X. Fan, Y. Tao, C. Deng, K. Yu, W. Zhang, L. Deng, W. Xiong, Two-step freezing polymerization method for efficient synthesis of high-performance stimuli-responsive hydrogels. *ACS Omega* **5**, 5921–5930 (2020).
45. S. D. Rezaei, S. Shannigrahi, S. Ramakrishna, A review of conventional, advanced, and smart glazing technologies and materials for improving indoor environment. *Sol. Energy Mater. Sol. Cells* **159**, 26–51 (2017).
46. World Wide Travel Organisation, World Weather & Climate Information *Weather-and-Climate* (2021); <https://weather-climate.com/>.
47. Thermostats. U.S. Department of Energy, [www.energy.gov/energysaver/thermostats](http://www.energy.gov/energysaver/thermostats).
48. Internal heat gains in relation to living area. *The Passive House Resource*, [https://passipedia.org/planning/calculating\\_energy\\_efficiency/phpp\\_-\\_the\\_passive\\_house\\_planning\\_package/internal\\_heat\\_gains\\_in\\_relation\\_to\\_living\\_area](https://passipedia.org/planning/calculating_energy_efficiency/phpp_-_the_passive_house_planning_package/internal_heat_gains_in_relation_to_living_area).
49. C. U. Ibeji, J. Adegboyega, O. D. Okagu, B. B. Adeleke, Nature of ground state of benzophenone and some of its substituted derivatives: Experimental and DFT study. *J. Appl. Sci.* **16**, 504–516 (2016).
50. International Organization for Standardization, Thermal performance of windows, doors, and shading devices – Detailed calculations. *ISO 15099:2003* (2003).
51. E. U. Finlayson, D. K. Arasteh, C. Huijenga, M. D. Rubin, M. S. Reilly, No title. *WINDOW 4.0: Documentation of Calculation Procedures* (Energy and environment division, Lawrence Berkeley laboratory, University of California, 1993).

## Acknowledgments

**Funding:** We are thankful for the financial support from the Hong Kong General Research Fund (grant nos. 16206020 and 16210021) and Smart Sensors and Environmental

Technologies (grant no. IOPCF21EG01) in the Hong Kong University of Science and Technology. This work was also supported in part by the Project of Hetao Shenzhen-Hong Kong Science and Technology Innovation Cooperation Zone (HZQB-KCZYB-2020083) and the Environment and Conservation Fund (ECF Project 119/2020).

**Author contributions:** Conceptualization: C.L., B.H., and J.H. Fabrication: C.L. and J.H. Characterization: C.L., J.H., and G.L. Experiment: C.L. and J.H. Simulation: C.L. Analysis: C.L., J.H., and W.L. Suggestion: C.Y.H.C., S.Y., W.L., and B.H. Writing—original draft: C.L. Writing—review and editing: C.L., J.H., S.Y., W.L., and B.H. **Competing interests:** C.L., J.H., S.Y., and B.H. are inventors on a provisional patent application related to this work filed by The Hong Kong University of Science and

Technology (no. 63/282,668; filed 23 November 2021). The authors declare that they have no other competing interests. **Data and materials availability:** All data needed to evaluate the conclusions in the paper are present in the paper and/or the Supplementary Materials.

Submitted 16 December 2021

Accepted 14 March 2022

Published 29 April 2022

10.1126/sciadv.abn7359

## All-weather thermochromic windows for synchronous solar and thermal radiation regulation

Chongjia LinJun HurChristopher Y. H. ChaoGongze LiuShuhuai YaoWeihong LiBaoling Huang

*Sci. Adv.*, 8 (17), eabn7359. • DOI: 10.1126/sciadv.abn7359

### View the article online

<https://www.science.org/doi/10.1126/sciadv.abn7359>

### Permissions

<https://www.science.org/help/reprints-and-permissions>